Journal of the Mechanical Behavior of Biomedical Materials 77 (2018) 321–330

Contents lists available at ScienceDirect

Journal of the Mechanical Behavior of Biomedical Materials

journal homepage: www.elsevier.com/locate/jmbbm

Experimental and numerical studies of two arterial wall delamination modes

Xiaochang Leng[a,*], Boran Zhou[b], Xiaomin Deng[c], Lindsey Davis[d], Susan M. Lessner[d,e], Michael A. Sutton[c,d], Tarek Shazly[c,d]

[a] Institute of Engineering Mechanics, Nanchang University, Jiangxi 330031, People's Republic of China
[b] Department of Radiology, Mayo Clinic, Rochester, MN 55905, United States
[c] College of Engineering and Computing, Department of Mechanical Engineering, University of South Carolina, Columbia, SC 29208, United States
[d] College of Engineering and Computing, Biomedical Engineering Program, University of South Carolina, Columbia, SC 29208, United States
[e] School of Medicine, Department of Cell Biology & Anatomy, University of South Carolina, Columbia, SC 29208, United States

ARTICLE INFO

Keywords:
Vascular mechanics
Delamination
Cohesive zone model
Holzapfel-Gasser-Ogden model
Energy release rate
Mixed-mode

ABSTRACT

Arterial wall dissection, which results from various pathophysiological processes, can lead to the occurrence of large area delamination in the aortic wall that can potentially block blood flow and lead to deleterious clinical conditions. Despite its critical clinical relevance, few studies have focused on investigating the failure mode of delamination in the arterial wall. In this study, we quantify the energy release rate of the medial layer of a porcine abdominal aorta via two delamination experiments: the mixed-mode delamination experiment and the "T"-shaped delamination experiment. A cohesive zone model (CZM) is applied to simulate the arterial wall delamination and Holzapfel-Gasser-Ogden (HGO) material model is used to capture the bulk arterial material behavior. A set of parameter values for the HGO and CZM models are identified through matching simulation predictions of the load vs. load-point displacement curve with experimental measurements. Then the parameter values and critical energy release rates obtained from experiments are used as input data for simulation predictions for two arterial wall delamination experiments. The simulation predictions show that the delamination front matches well with experimental measurements. Moreover, the mixed-mode delamination experiment reveals a shear mode-dominated failure event, whereas the "T"-shaped delamination experiment is an opening failure process. The integration of experimental data and numerical predictions of arterial delamination events provides a comprehensive description of distinct failure modes and aids in the prediction of aortic dissection.

1. Introduction

Aortic dissection, manifested as delamination and separation of the medial layer of the arterial wall, may result in significant blood flow directed into the newly created second lumen. The diverted blood flow further promotes the delamination process in the form of Mode I or Mixed-mode failure (Gasser and Holzapfel, 2006; Leng et al., 2015a). Moreover, with the inherent inhomogeneity of the arterial wall along the delamination path, the delaminated medial layer may be peeled from the other layers by a mixed-mode failure process (Leng et al., 2015a). The failure process within the media can trigger aortic dissection and may cause rupture of abdominal aortic aneurysms (Daugherty and Cassis, 2002; Golledge and Norman, 2010; Venkatasubramaniam et al., 2004) and false lumen patency of descending thoracic aorta (Bernard et al., 2001). Numerous studies have investigated the dissection behavior of arterial tissue under mode I (Ferrara and Pandolfi, 2010; Gasser and Holzapfel, 2006) or mixed-mode failure between atherosclerotic plaque and media (Leng et al., 2015a), yet little research has focused on comparing the contributions of these two failure modes to the delamination propagation process in the arterial wall.

It is well known that elastin is the major load bearing structural component of the arterial wall at low strain and that collagen fibers contribute to the stiffening of the arterial tissue at high strain as they are gradually recruited (Ferrara and Pandolfi, 2010; Zhou et al., 2015). Structurally motivated constitutive models of arterial tissue specifically account for the distinct mechanical behaviors of these two matrix proteins in determining the overall material response over a wide range of physiological loads. In particular, the Holzapfel-Gasser-Ogden (HGO) material model has been widely employed for modeling the mechanical properties of arterial walls and characterizing the local stress environment of mechano-sensitive vascular smooth muscle cells in the arterial wall under large deformations (Ferrara and Pandolfi, 2010; Leng et al., 2015a; Prim et al., 2016).

* Correspondence to: 999 University Avenue, Honggutan District, Nanchang, Jiangxi 330031, People's Republic of China.
E-mail address: lengxc1984@163.com (X. Leng).

http://dx.doi.org/10.1016/j.jmbbm.2017.09.025
Received 18 May 2017; Received in revised form 11 September 2017; Accepted 15 September 2017
Available online 19 September 2017
1751-6161/ © 2017 Published by Elsevier Ltd.

The cohesive zone model (CZM) provides an effective method for modeling the interfacial damage within the arterial wall during the delamination processes. Numerous studies have employed the CZM approach to characterize interfacial debonding and delamination processes in fiber-reinforced composite materials (Roy and Dodds, 2001; Turon et al., 2006). This method has also been implemented to study the failure of arterial tissue in two- (Ferrara and Pandolfi, 2010; Gasser and Holzapfel, 2006) and three-dimensions (Gasser and Holzapfel, 2007; Leng et al., 2015a). Moreover, the CZM with an exponential cohesive law has been adopted for modeling the delamination behavior along the interface within the medial layer of porcine abdominal aorta (Camanho et al., 2003).

Existing studies in the literature have investigated the dissection of the arterial wall, but experimental investigations of arterial wall delamination events and the analyses and numerical simulations of such events have been limited. The objectives of this study are two-fold. First, an integrated experimental-computational approach is applied to study two forms of failures in porcine abdominal aorta specimens, quantifying the interfacial strength and critical energy release rate of the interface within the media via the CZM approach. The CZM method is validated by comparisons of the predicted loading-delamination-unloading curves and the predicted distances from the delamination front to the initial front with experimental measurements.

2. Materials and methods

2.1. Experimental procedure

The delamination experimental protocol in this study follows that used in our previous studies (Wang et al., 2013, 2014, 2011). One set of intact kidneys was obtained from the local slaughterhouse, rinsed in iced phosphate-buffered saline (PBS) solution and transported back to the laboratory. The abdominal aorta was isolated from the surrounding tissues, washed in PBS and dissected from the perivascular tissue. An approximately 30 mm long segment was cut, following a radial cut imposed onto the sample along the vessel axis, yielding a strip. Two groups of specimens oriented at the angle of 0° and 90°, respectively, with respect to the circumferential vessel axis were cut from porcine aortas (Fig. 1).

There are 12 specimens for each group. Six specimens oriented at the angle of 0° with respect to the circumferential vessel axis were used for the mixed-mode delamination experiment and the other six specimens were used for the “T” delamination experiment. These specimens are said to be oriented in the circumferential direction.

The same two types of experiments were also performed on twelve specimens oriented at an angle of 90° with respect to the circumferential vessel axis, as shown in Fig. 1. These specimens are said to be oriented in the axial direction.

In each case, to initiate a delamination process in the medial layer of the arterial wall, a small initial delamination (5 mm long) with a straight front was carefully introduced at one end of the specimen inside the medial layer.

In the “mixed-mode” experiment (see Fig. 3a and c), the bottom surface of the lower portion of the specimen was glued to a glass plate in order to restrict its motion during loading, and the proximal end of the upper delaminated portion was peeled away by a micro-clamp. During the delamination process, the delaminated upper portion became almost parallel to the lower portion and to the not-yet delaminated interface (Fig. 3c).

In the “T”-shaped delamination experiment (see Fig. 3b and d), the proximal end of one of the two initially separated portions of the specimen was fixed by tissue glue to a glass plate and the proximal end of the other separated portion was pulled away by a micro-clamp. During the delamination process, the two delaminated portions stay parallel to each other but are approximately perpendicular to the not-yet delaminated interface (Fig. 3d).

During each experiment, the prescribed displacement and reaction load were recorded via the system actuator and load cell (Bose ELF 3200, Biodynamic Co, MN). The delamination process was recorded by a computer vision system in which two cameras were perpendicularly positioned to get both front and side views of the specimen.

For each experiment, the recorded reaction load and the prescribed displacement data are presented in the form of a load vs. displacement curve (e.g. see Fig. 4). Each curve consists of several cycles, and the curve for each cycle contains a loading phase, a delamination phase, and an unloading phase.

3. Theoretical framework

3.1. HGO model

The HGO model assumes that collagen fibers are oriented parallel to the arterial wall at a certain angle with respect to the vessel axis (Gasser et al., 2006; Holzapfel et al., 2000). The mechanical response of the arterial wall at low strain is governed by the amorphous matrix, while as strain increases, two families of collagen fibers are gradually recruited and begin to take up the load, contributing to the highly nonlinear mechanical behavior of the arterial tissue. The strain energy potential per unit reference volume in a decoupled form is given by:

$$\Psi(\boldsymbol{C}, \boldsymbol{H}_1, \boldsymbol{H}_2) = \Psi_{vol}(J) + \overline{\Psi}(\overline{\boldsymbol{C}}, \boldsymbol{H}_1, \boldsymbol{H}_2) \tag{1}$$

where $\boldsymbol{C}$ is the right Cauchy-Green strain tensor and $\overline{\boldsymbol{C}}$ denotes a modified counterpart, $\overline{\boldsymbol{C}} = \overline{\boldsymbol{F}}^T\overline{\boldsymbol{F}}$; $\overline{\boldsymbol{F}} = J^{-1/3}\boldsymbol{F}$, $\boldsymbol{F}$ is the deformation gradient tensor and $J = \det(\boldsymbol{F})$. The volumetric part, $\Psi_{vol}(J)$, is given by (ABAQUS, 2013),

$$\Psi_{vol}(J) = \frac{1}{D}\left(\frac{J^2-1}{2} - InJ\right) \tag{2}$$

where $\frac{1}{D}$ is analogous to the elastic modulus of the material.

The free-energy function $\overline{\Psi}$ (Gasser et al., 2006), is expressed as

$$\overline{\Psi}(\overline{\boldsymbol{C}}, \boldsymbol{H}_1, \boldsymbol{H}_2) = \frac{\mu}{2}(\overline{I}_1-3) + \frac{k_1}{2k_2}[e^{k_2[\kappa\overline{I}_1+(1-3\kappa)\overline{I}_{41}-1]^2}-1] + \frac{k_1}{2k_2}[e^{k_2[\kappa\overline{I}_1+(1-3\kappa)\overline{I}_{42}-1]^2}-1] \tag{3}$$

where μ is a parameter having the dimension of stress and representing the shear modulus of the amorphous matrix; $\overline{I}_1 = tr(\overline{\boldsymbol{C}})$ is the first invariant of $\overline{\boldsymbol{C}}$; k_1 denotes the relative stiffness of fibers; k_2 is a dimensionless parameter; $\overline{I}_{41}$ and $\overline{I}_{42}$ are tensor invariants equal to the square of the stretch in the direction of two families of fibers, respectively; $\boldsymbol{I}$ is the identity tensor; and κ is the dispersion parameter, describing the dispersion of the two families of fibers. $\kappa = 0$ when the two collagen fiber families are parallel to each other and $\kappa = 1/3$ when the collagen fibers distribute isotropically; γ denotes the angle between the mean fiber orientation of one family of fibers and the circumferential direction of the aorta.

3.2. Interface damage model

In this study, the CZM approach is employed to represent the interfacial behavior and to characterize interfacial damage in order to model arterial delamination failure. An exponential cohesive traction-separation law is used, which is implemented in the commercial finite element software ABAQUS 6.13 (Dassault Systèmes, France) through a user-defined UEL subroutine. As shown in Fig. 2b, δ_n and δ_s denote the displacement jumps (separation) normal and tangent to the cohesive surfaces, respectively. The sliding displacement δ_s across the cohesive surfaces can be calculated in the form (Ortiz and Pandolfi, 1999)

$$\delta_s = \sqrt{\delta_{s1}^2 + \delta_{s2}^2} \tag{4}$$

where δ_{s1} (the shearing displacement) and δ_{s2} (the tearing displacement)

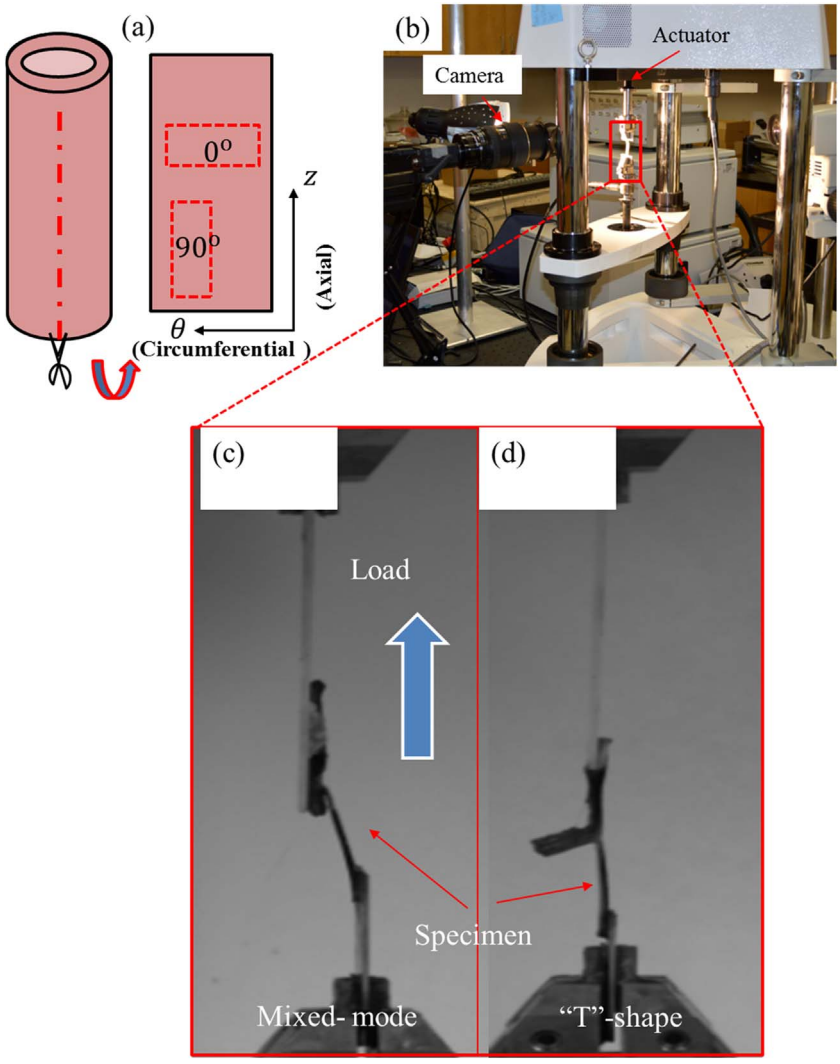

Fig. 1. Schematic of experimental setup. (a) A longitudinal cut was made on the porcine abdominal aorta and strips oriented at the angle of 0° and 90° with respect to the circumferential vessel axis were obtained; (b) Experimental setup of delamination experiments; (c) mixed-mode and (d) “T”-shaped delamination experiment setup (zoomed-in view).

denote the two perpendicular components of the sliding displacement (δ_s) in tangential directions across the cohesive surfaces.

The effective displacement jump is calculated as follows,

$$\delta = \sqrt{\lambda^2\delta_s^2 + \delta_n^2}. \tag{5}$$

where λ is a scalar parameter which is introduced to assign different weights to the opening (normal) displacement δ_n and sliding (tangent) displacement δ_s. Similarly, let t_n, t_{s1} and t_{s2} be the normal and two shear tractions across the cohesive surfaces, respectively. The effective traction is calculated as follows (Ortiz and Pandolfi, 1999),

$$t = \sqrt{\lambda^{-2}(t_{s1}^2 + t_{s2}^2) + t_n^2}, \tag{6}$$

The local effective traction of the exponential CZM in the loading condition is calculated as (Ortiz and Pandolfi, 1999; Roy and Dodds, 2001),

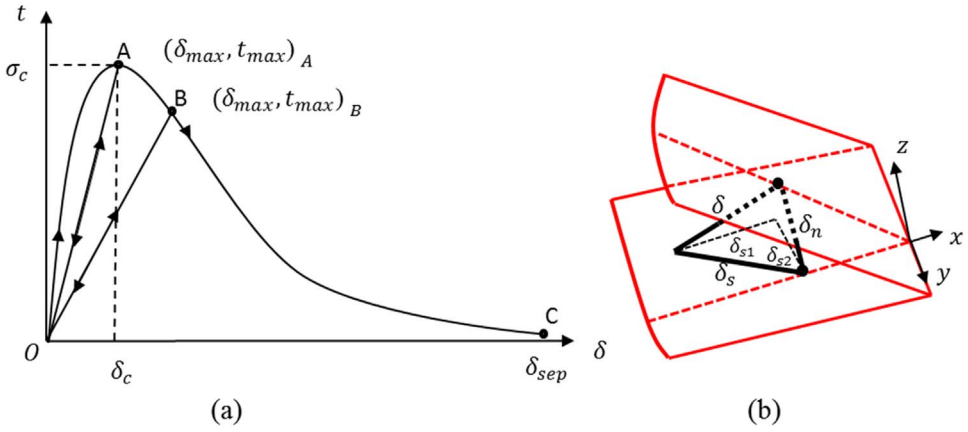

Fig. 2. (a) Effective traction vs. effective displacement jump curve in the irreversible exponential cohesive zone model; (b) a schematic of sliding (δ_s), opening (δ_n) and effective (δ) displacement jumps.

$$t = e\sigma_c \frac{\delta}{\delta_c} exp\,(-\frac{\delta}{\delta_c}) \quad \text{if} \quad \delta \geq \delta_{max} \quad \text{or} \quad \dot{\delta} \geq 0; \quad t_n = K\delta_n \quad \text{if} \quad \delta_n < 0 \tag{7}$$

where $e = \exp(1) \approx 2.71828$ and σ_c denotes the strength of the material; $\delta_c = \frac{G_c}{e\sigma_c}$ is the maximum effective displacement at $t = \sigma_c$; δ_{sep} is the effective displacement when the cohesive interface element is completely damaged (i.e., when the element fails), and K is the penalty stiffness of penetration resistance to handle the artificial situation of cohesive surface inter-penetration when the opening displacement jump becomes negative.

During the unloading process, the local effective traction of the CZM (Ortiz and Pandolfi, 1999) is calculated as,

$$t = \left(\frac{t_{max}}{\delta_{max}}\right)\delta \quad \text{if} \quad \delta < \delta_{max} \quad \text{or} \quad \dot{\delta} < 0 \tag{8}$$

where δ_{max} denotes the maximum effective displacement jump during one delamination cycle, and t_{max} is the corresponding effective traction. The work of separation per unit cohesive surface area follows the form:

$$G_c = e\sigma_c\delta_c \tag{9}$$

Following the reference (Ortiz and Pandolfi, 1999), and based on the displacement jump definition given in (4) and (5), a parameter d, representing the damage of the cohesive surfaces during the loading process, is introduced as follows:

$$d = 1 - \left(1 + \frac{\delta_{max}}{\delta_c}\right) exp\,(-\frac{\delta_{max}}{\delta_c}) \tag{10}$$

The parameter d ranges from 0 to 1, corresponding to the state of damage of the cohesive surfaces. Fig. 2 illustrates the loading and unloading processes of the cohesive traction-separation law, which shows the damage accumulated with the effective traction t. Thus, the force-displacement relation goes along line AO and BO when unloading at point A or B, respectively, because permanent damage occurs on the cohesive surface at point A or B.

4. Numerical implementation

Simulation of the arterial delamination process was implemented via the general-purpose finite element software ABAQUS 6.13 (ABAQUS, 2013). The mechanical data in terms of the load vs. displacement curve from the first cycle of the media delamination experiment was used to identify the HGO and CZM model parameter values. Simulations of the loading-delamination-unloading processes for subsequent cycles were performed, in which the set of HGO and CZM parameter values identified from the first cycle were used. Validation of the CZM-based approach was achieved by comparing simulation predictions of the load-displacement curves and of the distances from delamination front to the initial front with experimental measurements for the subsequent cycles.

4.1. Finite element model

The images (Fig. 3a, b) taken during the experiments were used to reconstruct the specimen geometry (Fig. 3c, d). The delamination areas during a delamination experiment were quantified directly from the experimental images taken at different times during an experiment.

4.1.1. Meshing

The arterial wall was meshed with eight-node brick elements (C3D8H). The cohesive interface is meshed with zero-thickness eight-node 3D user-defined elements, which were placed along the delamination path starting from the initial delamination front to the end of the media. The global size of the element for arterial wall is 0.4 mm and the cohesive element size is 0.1 mm, as shown in Fig. 3.

4.1.2. Boundary conditions

At the beginning of the mixed-mode delamination experiment, the bottom surface of the lower portion of the specimen was fixed and displacement loading was applied to a certain area of the proximal end of the upper delaminated portion, causing delamination at the media layer (Fig. 3a, c). For the "T"-shaped delamination experiment, the proximal end of one of the two initially separated portions of the specimen was fixed and the proximal end of the other separated portion was pulled away, causing delamination at the media layer (Fig. 3b, d). The displacement loading rate in the experiments was prescribed as 0.05 mm/s.

4.2. Identification of material parameters for HGO model

The material parameter values associated with the HGO model for aortic layers and the CZM for the delamination interface were identified by matching simulation predictions of the load-displacement curve from the loading phase and the delamination phase with experimental measurements of the mixed-mode and "T"-shaped delamination experiments (Fig. 4) (Chen et al., 2013; Leng et al., 2015a).

In this study, the criteria for identifying material parameter values associated with the HGO and CZM models was based on the root of mean square error (Zhou et al., 2015, 2014),

$$\varepsilon = \frac{\sqrt{\frac{\chi^2}{n-q}}}{F_{ref}} < 0.15, \chi^2 = \sum_{i=1}^{n} [(F_{exp} - F_{sim})_i^2] \tag{11}$$

where F_{exp} and F_{sim} are the experimentally measured and simulation predicted forces, respectively; F_{ref} is the mean value of the force over all data points; n is the total number of data points distributed over the delamination cycles that were used for the parameter identification process; q is the number of parameters for the HGO model. A set of identified HGO parameter values for the mixed-mode ($\varepsilon = 0.104$, $N = 68$, $q = 6$) and "T"–shaped ($\varepsilon = 0.078$, $N = 71$, $q = 6$) delamination experiments are shown in Table 1.

4.3. Material parameters associated with the CZM

In the current study, two failure processes, mixed-mode and "T"-shaped delamination, were investigated. The values of the critical energy release rates of the arterial tissue from the experiments (see Section 2.1) were quantified, and the CZM parameters K and λ were chosen from the literature (Leng et al., 2015a). The material property identification process mentioned in Section 4.2 was used to determine the interfacial strength σ_c for the CZM model through matching simulation predictions of the delamination phase of the load-displacement curve from cycle 1 with experimental measurements. Those values are shown in Table 2.

5. Results

5.1. Arterial tissue delamination

The delamination behavior of porcine abdominal aorta tissue was assessed via quasi-static tissue peeling tests, generating mechanical data in terms of load-displacement relationships, which were characterized by the jagged plateau regions (Figs. 5 and 6). The distances of positions for the start and the end of the delamination phase from point O in one loading-delamination-unloading cycle were represented by a_0 and a_e, respectively. The distances from the load point to the point O corresponding to the delamination fronts a_0 and a_e were represented by l_0 and l_e, respectively (Fig. 5a, b).

Fig. 5 shows the load/width (i.e. load per unit specimen width) vs. load-point displacement curves for the mixed-mode delamination experiments, in which Fig. 5a and b are for specimens oriented,

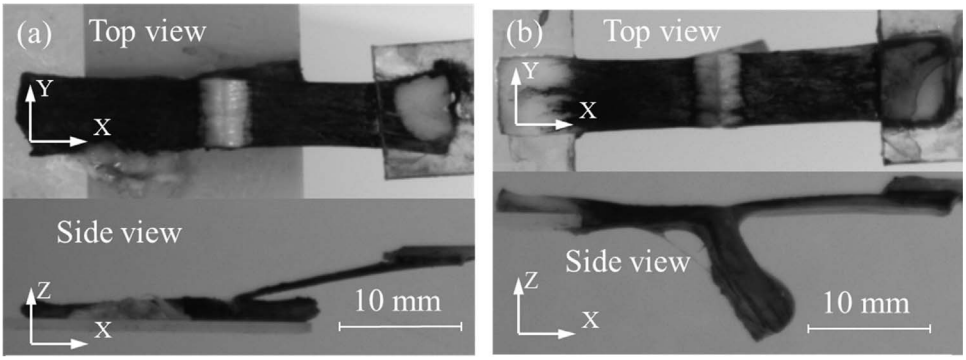

Fig. 3. Images of (a) mixed-mode and (b) "T" delamination experiments on porcine abdominal aorta specimens, and deformed shapes of (c) mixed-mode and (d) "T"-shaped delamination specimens from finite element simulations. The right delaminated part of the specimen (red section) contains intima and part of media, and the left delaminated part (blue section) contains adventitia and part of media. The delamination of aorta propagated inside the media layer. (For interpretation of the references to color in this figure legend, the reader is referred to the web version of this article.)

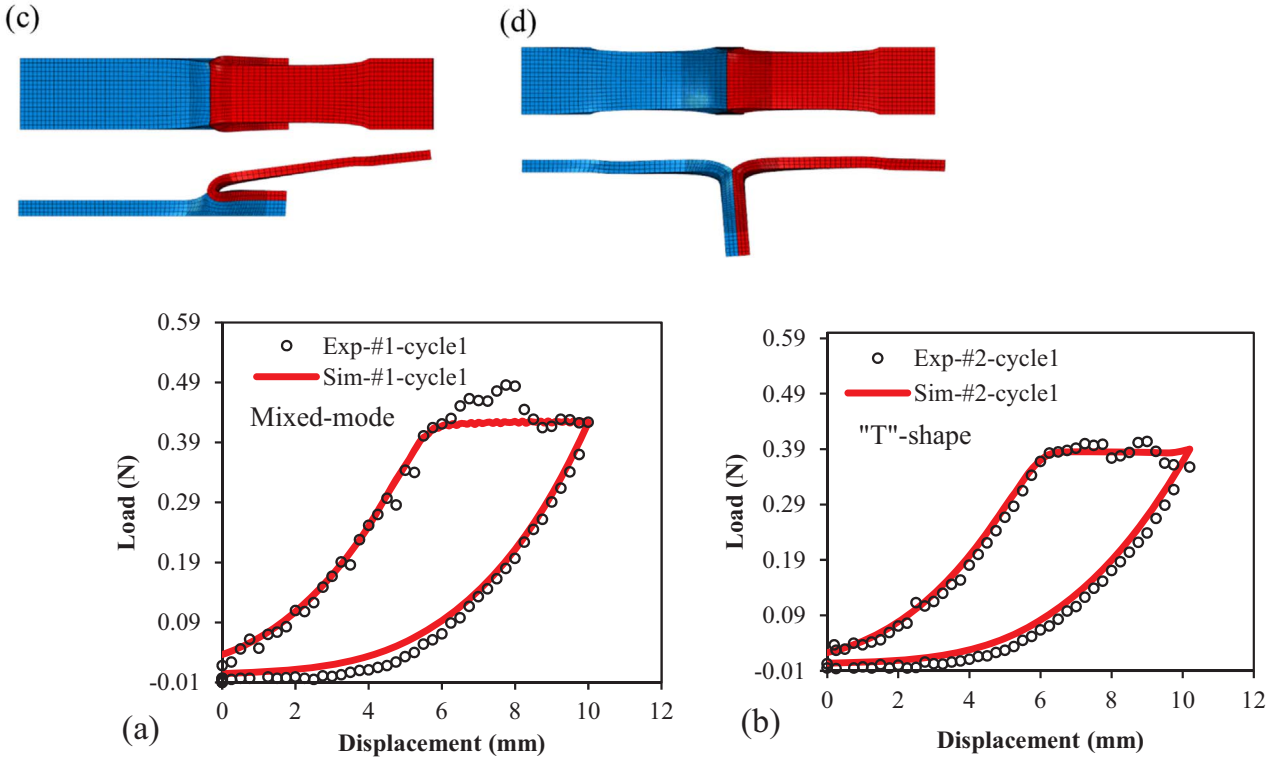

Fig. 4. The predicted load-displacement curves of one loading- delamination-unloading cycle are compared with the measured curves. (a) mixed-mode delamination experiment; (b) "T"-shaped delamination experiment.

Table 1
Material parameter values of HGO model.

	μ (kPa)	k_1 (kPa)	k_2	κ	γ (deg)
Mixed-mode	40	350	0.8	0.226	49
"T"-shape	40	500	0.8	0.226	45

Table 2
CZM parameter values.

CZM parameters	G_c (N/mm)	σ_c (MPa)	K (N/mm)	λ
Mixed-mode	0.22	0.44	1	1
"T"-shape	0.186	0.44	1	1

respectively, in the circumferential and axial directions (see Fig. 1a). Similarly, Fig. 6 shows the load/width vs. load-point displacement curves for the "T"-shaped delamination experiments, in which Fig. 6a and b are for specimens oriented, respectively, in the circumferential and axial directions.

Two observations can be made. First, the arithmetic means of the load/width vs. load-point displacement curves in Figs. 5a, b, 6a and b are approximately the same. Second, the distributions of the force/width for the axial specimens (0.042–0.095 N/mm and 0.042–0.082 N/mm for mixed-mode and "T"-shaped experiments, respectively) fall within a larger range than those for the circumferential specimens (0.048–0.079 N/mm and 0.044–0.073 N/mm for mixed-mode and "T"-shaped experiments, respectively) (Figs. 5 and 6).

An important mechanical property that can be measured from the delamination experiments is the energy release rate, G_c. The average values of the energy release rate with their related standard deviations (mean ± S.D.) for the circumferential and axial strip specimens under mixed-mode and "T"-shaped delamination are shown in Table 3.

For circumferential strip specimens, the arithmetic mean of G_c for the mixed-mode experiment (0.167 ± 0.036, mean ± SD, n = 6) is larger than that of the "T"-shaped experiment (0.151 ± 0.037, mean ± SD, n = 6). For axial strip specimens, the arithmetic mean of G_c for the mixed-mode experiment (0.19 ± 0.072, mean ± SD, n = 6) is also larger than that of the "T"-shaped experiment (0.165 ± 0.083, mean ± SD, n = 6). However, these differences are not statistically significant. Moreover, the arithmetic mean of the energy release rate for

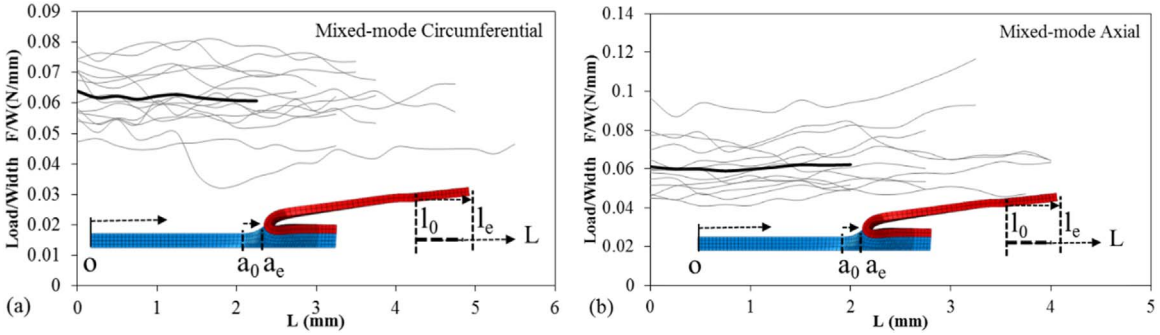

Fig. 5. Load/width versus load-point displacement curves for 6 circumferential and 6 axial strip specimens of mixed-mode delamination experiments. The light gray lines and thick black curves represent the measurements for specimens for each case and arithmetic mean values, respectively.

axial specimens is larger than that for circumferential specimens from both mixed-mode and "T"-shaped delamination experiments, which is in accord with the characteristics of peeling tests from other literature (Tong et al., 2011).

5.2. Validation of the CZM approach

5.2.1. Validation of the load-displacement curves

In the previous sections, two finite element models were developed for the mixed-mode (specimen Mix-C1) and "T"-shaped (specimen MI-C2) aortic media delamination experiments, and the parameter values for the HGO model and for the exponential CZM were identified. This section will focus on the prediction of the load vs. load-point displacement curve, which can be used as a validation of the CZM- based modeling approach for porcine aortic media delamination processes through comparisons with experimental measurements of cycle 2 and cycle 3 for mixed-mode and "T"-shaped delamination experiments.

Simulation predictions of the load-displacement curves for cycle 2 (G_c = 0.219 N/mm) and cycle 3 (G_c = 0.205 N/mm) of the mixed-mode delamination experiment are shown in Fig. 7ab and those for cycle 2 (G_c = 0.191 N/mm) and cycle 3 (G_c = 0.161 N/mm) of the "T"-shaped delamination experiment are shown in Fig. 7cd, respectively. The overall simulation predictions match well with the experimental data, especially the loading phases of cycle 2 and cycle 3 for mixed-mode delamination.

5.2.2. Validation through the delamination fronts

In the previous section, the comparison of simulation predictions of the load vs. load-point displacement curves with the experimental measurements was taken as a way to validate the CZM-based approach. In the current section, the simulation predictions of the delaminated fronts for each cycle of mixed-mode and "T"-shaped delamination are used for comparison with those from experimental measurements to provide another validation for the CZM modeling approach. It is noted that, for the mouse plaque delamination (Leng et al., 2015a) and human fibrous cap delamination (Leng et al., 2015b), the delamination fronts were not recorded during the delamination process. So, it was not possible in those earlier studies to compare the predicted delamination fronts with those from experimental measurements.

At steady-state propagation conditions, the delamination fronts move forward with the separation of two aortic layers. Fig. 8 compares the total delamination distances from cycle 1 to cycle 3 with respect to the initial crack front for mixed-mode (Fig. 8a) and "T"-shaped experiments (Fig. 8b), respectively. The distance from one lateral side to the opposite side along the width direction is characterized by W and the distance from the initial crack front to that of the last time point of the delamination phase of one cycle is represented by *a*. It can be seen that the overall simulation predictions of delamination fronts match reasonably well with the experimental data for each cycle.

5.3. Ratios of $(\delta_{s1}/\delta)^2$ and $(\delta_n/\delta)^2$

In the literature, the mixed-mode delamination experiment described in this study is commonly called a peeling experiment, which is usually performed on specimens made of engineering materials and is a Mode I-dominated failure process. In the current study, however, the specimen is made of a biological tissue material and it is found that the delamination is not a Mode I-dominated process, which is why the experiment is called a mixed-mode experiment. It is found that the delamination of soft biological tissue involves a large sliding (shearing) displacement component along the delamination front. In particular, it is observed that the ratio of $(\delta_{s1}/\delta)^2$ is approximately 0.8, which is four times the value of $(\delta_n/\delta)^2$(Fig. 9d,e), which means the shearing component of the displacement jump at the delamination front is more dominant than the normal component.

On the other hand, the ratios of $(\delta_{s1}/\delta)^2$ and $(\delta_n/\delta)^2$ for the "T"-shaped experiment are 0 and 1, respectively, indicating that the "T"-shaped delamination experiment is a pure opening separation process.

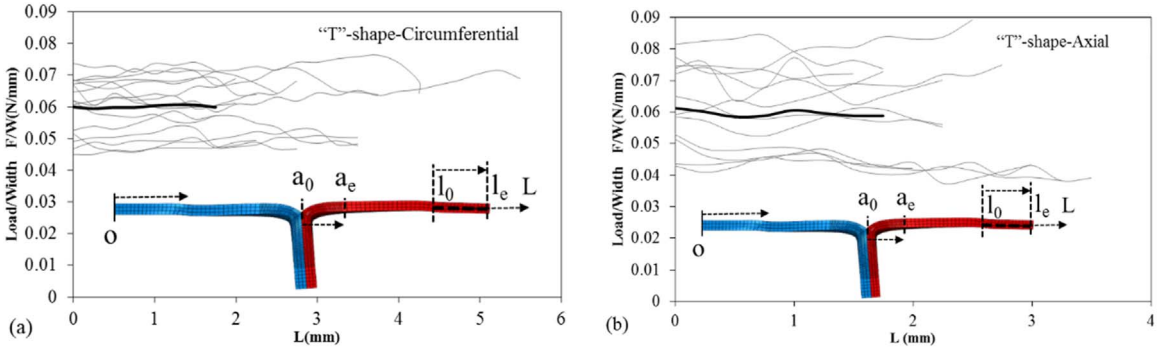

Fig. 6. Load/width versus load-point displacement curves for 6 circumferential and 6 axial strip specimens of "T"-shaped delamination experiments. The light gray lines and thick black curves represent the measurements for specimens for each case and arithmetic mean values, respectively.

Table 3
The values of energy release rate (G_c) for mixed-mode and "T"-shaped delamination of porcine aortic tissue: Mix-C1–Mix-C6, Mix-A1–Mix-A6, MI-C1–MI-C6 and MI-A1–MI-A6 are the specimens of mixed-mode and "T"-shaped delamination experiments from circumferential (C) and axial (A) directions, respectively.

Circumferential				**Axial**			
Mixed-mode		**"T"-shaped**		**Mixed-mode**		**"T"-shaped**	
Specimen	G(N/mm)	Specimen	G(N/mm)	Specimen	G(N/mm)	Specimen	G(N/mm)
Mix-C1	0.215 ± 0.007	MI-C1	0.19 ± 0.023	Mix-A1	0.166 ± 0.043	MI-A1	0.137 ± 0.04
Mix-C2	0.163 ± 0.033	MI-C2	0.179 ± 0.01	Mix-A2	0.329 ± 0.084	MI-A2	0.22 ± 0.014
Mix-C3	0.136 ± 0.022	MI-C3	0.111 ± 0.011	Mix-A3	0.137 ± 0.005	MI-A3	0.301 ± 0.096
Mix-C4	0.133 ± 0.004	MI-C4	0.184 ± 0.016	Mix-A4	0.14 ± 0.015	MI-A4	0.111 ± 0.029
Mix-C5	0.151 ± 0.003	MI-C5	0.123 ± 0.007	Mix-A5	0.227 ± 0.032	MI-A5	0.111 ± 0.008
Mix-C6	0.2 ± 0.01	MI-C6	0.126 ± 0.028	Mix-A6	0.172 ± 0.019	MI-A6	0.104 ± 0.008
Mean	0.167 ± 0.036		0.151 ± 0.037		0.19 ± 0.072		0.165 ± 0.083

Taking into account the loading angles (Fig. 10a) of the mixed-mode delamination, the ratio of $(\delta_n/\delta)^2$ increased with the loading angle whereas the ratio of $(\delta_{s1}/\delta)^2$ decreased with the loading angle. Moreover, the values of $(\delta_n/\delta)^2$ are larger at the mid-plane than at the outside surface, and the trend is reversed for the ratios of $(\delta_{s1}/\delta)^2$.

6. Discussion

The aim of this study is to quantify the delamination behavior of circumferential and axial strip specimens of porcine aorta using mixed-mode and "T"-shaped delamination experiments and to develop a mathematical formulation to model the arterial tissue delamination behavior. The experimental data were processed to calculate the energy release rate that describes the strength of the arterial tissue. A structure-motivated constitutive model (the HGO model) and a cohesive zone model (CZM) of the arterial tissue were proposed and verified to allow prediction of aortic media delamination events.

For the aortic media delamination experiments, the arithmetic means of load/width ratios are approximately 0.06 N/mm for all failure modes and specimen orientations, which are of the same order as the force/width ratios for delamination of human aortic media, 0.023 ± 0.003 N/mm and 0.035 ± 0.002 N/mm, derived from peeling tests of specimens oriented in the circumferential and axial directions, respectively (Sommer et al., 2008). The load/width value describes the

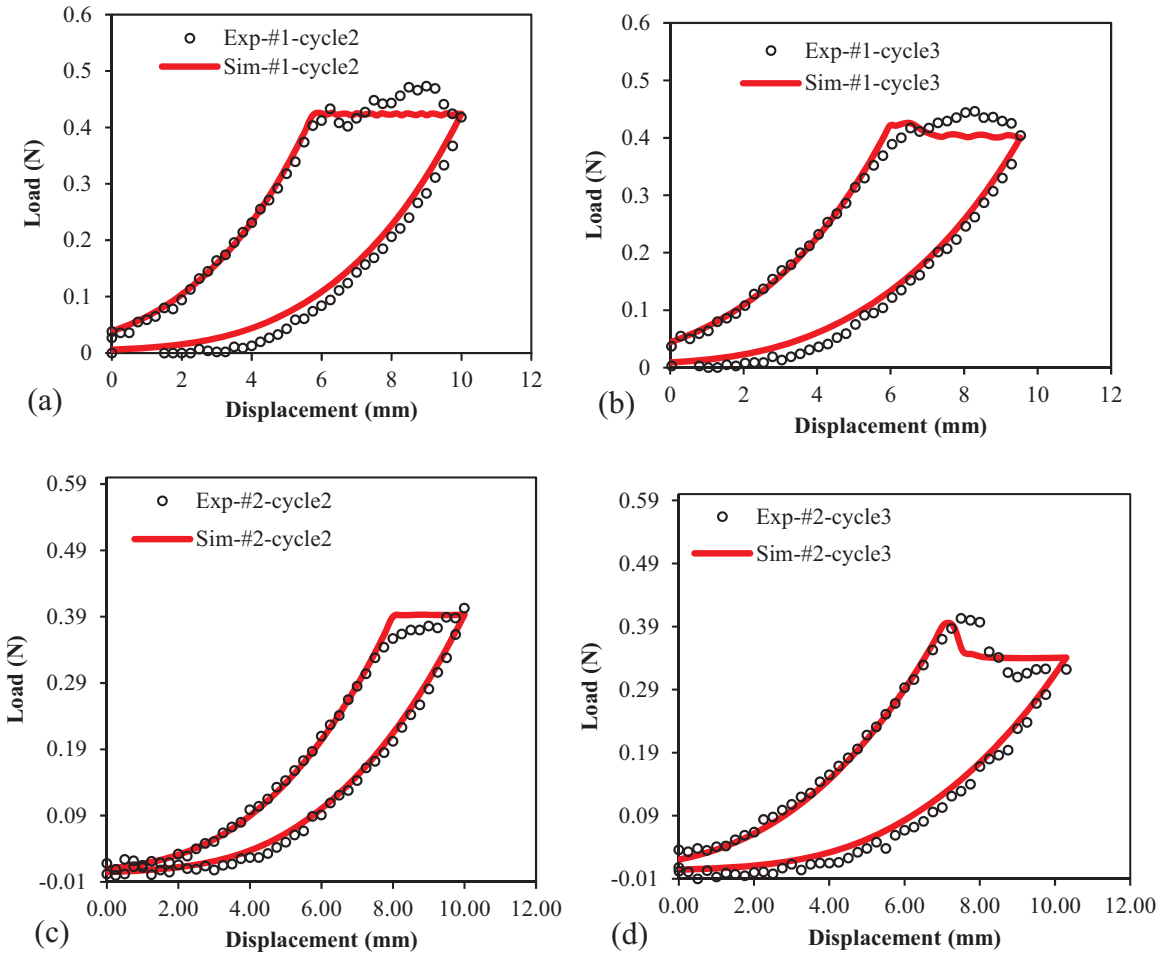

Fig. 7. The simulation predicted load-displacement curves of four loading-delamination-unloading cycles are compared with the experimentally measured curves, (a) cycle 2 and (b) cycle 3 of mixed-mode delamination; (c) cycle 2 and (d) cycle 3 of "T"-shaped delamination.

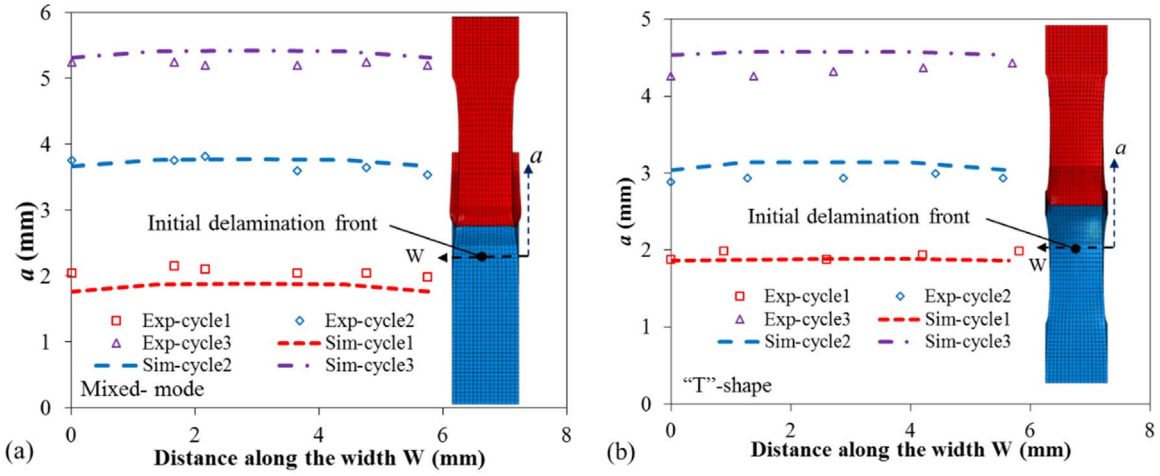

Fig. 8. Comparison of predicted and measured delamination front profiles: (a) mixed-mode experiment; (b) "T"-shaped experiment.

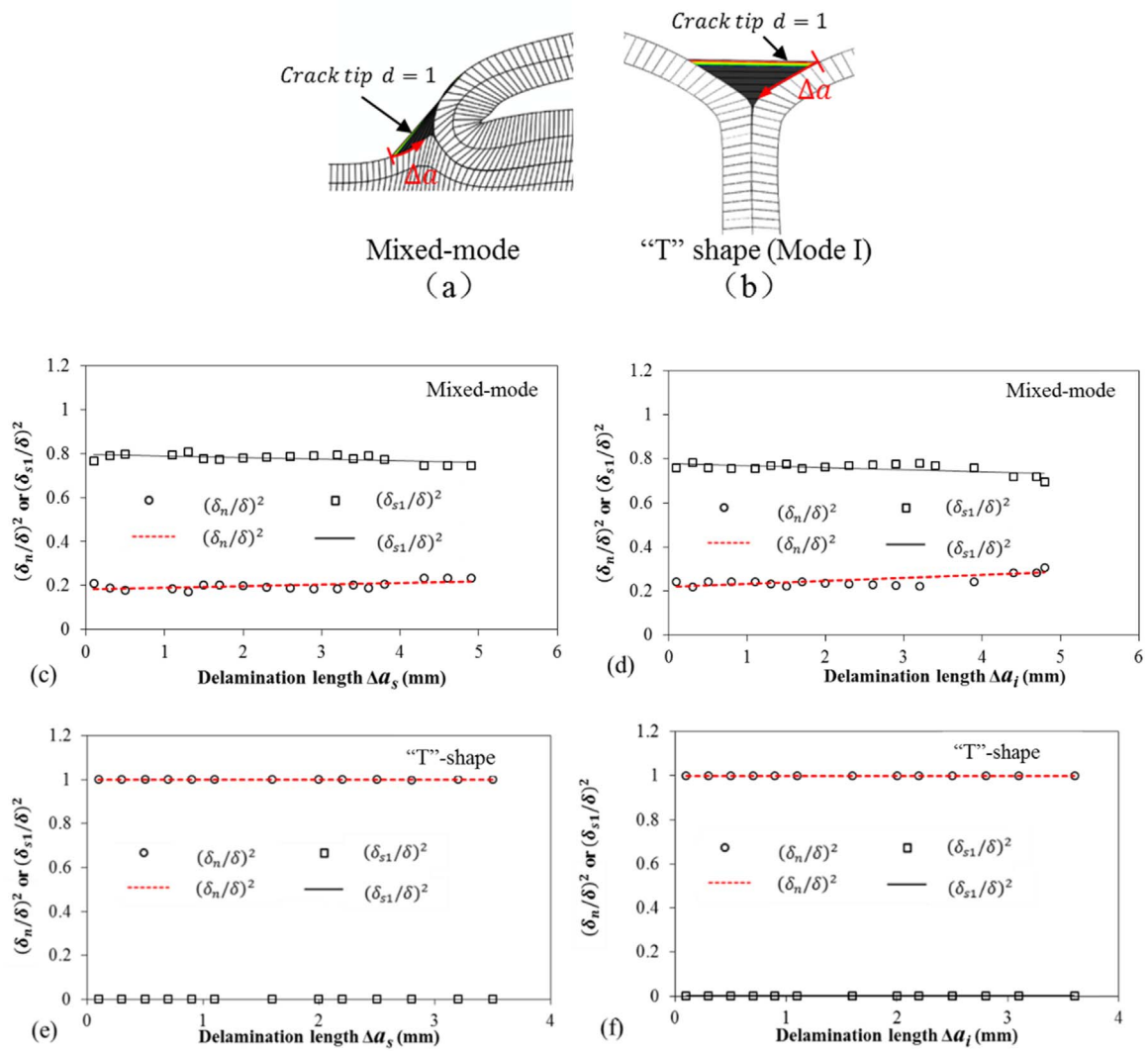

Fig. 9. Predicted ratios of $(\delta_n/\delta)^2$ and $(\delta_{s1}/\delta)^2$; the definition of delamination fronts (where damage parameter equals one) for (a) mixed mode and (b) "T"-shaped delamination; ratios of $(\delta_n/\delta)^2$ and $(\delta_{s1}/\delta)^2$ of delamination experiments for mixed mode (c) at the outside surface and (d) at the mid-plane as well as for "T"-shaped experiment (e) at the outside surface and (f) at the center plane, respectively.

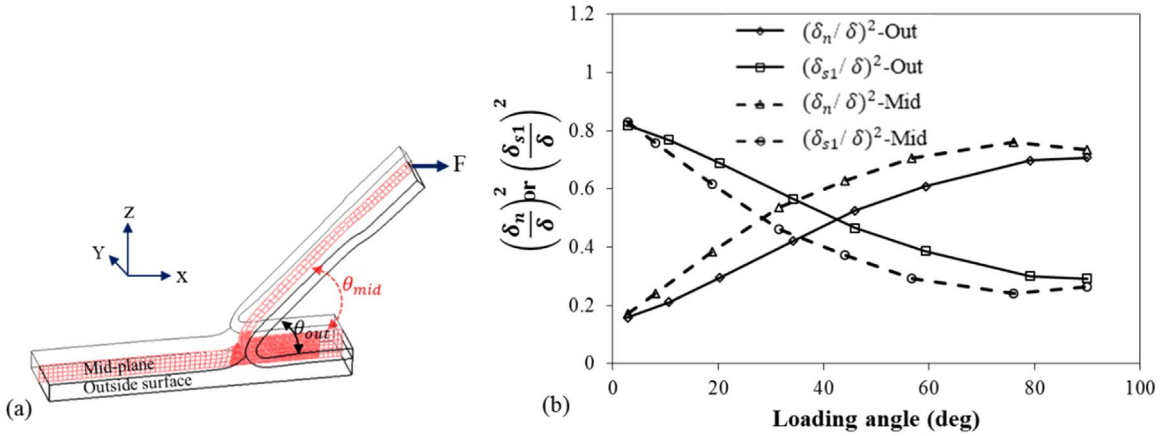

Fig. 10. (a) Loading angles at middle plane θ_{mid} and outside surface θ_{out}; (b) predicted ratios of $(\delta_{s1}/\delta)^2$ and $(\delta_n/\delta)^2$ related to loading angles for mixed-mode experiment.

load per unit width that causes the movement of the load point during delamination, which is resisted mainly by the collagen fibers. However, this value does not provide a criterion for determining the delamination mode.

The energy release rate represents the delamination toughness of a material when delamination failure initiates and propagates in the material, and is often taken as a critical parameter in establishing a delamination criterion. A number of studies have quantified the critical energy release rates for arterial material separation processes. In particular, the dissection energy per unit separation area for upper descending thoracic porcine aorta is 0.159 ± 0.009 N/mm (Carson and Roach, 1990), the energy/area for porcine abdominal aorta has a range from 0.019 ± 0.009 N/mm to 0.113 ± 0.004 N/mm (Roach and Song, 1994), and the dissection energies per area are 0.051 ± 0.006 N/mm and 0.076 ± 0.003 N/mm for circumferential and axial specimens of human aortic media (Sommer et al., 2008), respectively. The values of the critical energy release rate from the current porcine media delamination experiments (Table 3) are larger than many of those reported in the literature, but they are still within the range described above (Carson and Roach, 1990; Roach and Song, 1994; Sommer et al., 2008).

For the loading-delamination-unloading cycles of the load-displacement curves from the current delamination experiments that were used in the validation simulations, the comparisons between simulation predictions and experimental measurements show overall good agreement (see Fig. 7), though some differences in the comparisons are seen. in two regions. One region where there are slight differences is in the unloading phase of the load-displacement curve for the mixed-mode delamination experiment (see Fig. 7a and b), when the load is small. The other is in the delamination phase of the load-displacement curve.

There are two main factors that are expected to contribute to the observed differences between simulation predictions and experimental measurements. First, the specimen geometry is not regular and is reconstructed from images of the specimen, which involves approximations. In particular, approximations for the geometries of the specimen thickness and width (which are not uniform and vary with position in the specimen) will affect the accuracy of the predicted reaction load, especially at small loads. Regarding this effect, it is noted that the material model parameter values were identified from the cycle 1 load-displacement data and were applied in simulations to subsequent cycles. These loading cycles occur at different locations along the delamination path, which means that errors in the thickness approximations at different locations will affect the stress-strain response at these locations, leading to errors in the load-displacement predictions.

Secondly, the heterogeneous distribution of strong tissue components (e.g., collagen fibers) and relatively weak tissue components (e.g., elastin) is expected to lead to material property variations throughout the specimen, which can largely influence the local mechanical response and hence alter the load-displacement curve. However, in the simulations, a constant set of material model parameter values were used, which is expected to result in differences between simulation predictions and experimental measurements. In particular, the local composition of the aortic media, especially the extent of fiber bridging along the delamination path, plays an essential role in determining the local energy release rate. As a result, the critical energy release rate varies along the delamination path (see Table 3). In the current study, however, for either the mixed-mode or "T"-shaped delamination experiments, the simulations employed a constant input data for the critical energy release rate, which was the average of the measured energy release rates over all 3 cycles in each experiment.

To the authors' knowledge, the current study provides the first predictions of the delamination front in arterial tissue delamination. These predictions compare well with experimental measurements although some differences are observed (see Fig. 8). Reasons for the observed differences are believed to be the same as those discussed above for the load-displacement curve predictions.

The ratios of $(\delta_{s1}/\delta)^2$ and $(\delta_n/\delta)^2$ shown in Figs. 9 and 10 reveal that the "T"-shaped delamination experiment is an opening-mode (mode I) dominated failure process, and that the mixed-mode delamination experiment is a shearing-mode (mode II) dominated failure process when the loading angle is less than 28° at the middle plane and less than 41° at the outside surface of the specimen.

7. Conclusions

For both basic science and clinical studies, including those focused on disease diagnosis and risk evaluation, it is advantageous to understand the arterial delamination process under various loading conditions. A major goal of vascular biomechanics is to determine appropriate mathematical frameworks to describe tissue mechanical properties and interfacial strength, which allow for the solutions of boundary value problems with predictive power and high clinical relevance.

In the current study, two types of porcine aortic media delamination experiments were performed, the mixed-mode and "T"-shaped delamination experiments. A continuum mechanics modeling approach to simulate and understand these experiments was developed and validated. In particular, the use of the HGO model for arterial bulk material behavior and an exponential cohesive zone model for arterial interfacial behavior enabled the simulations of the aortic media delamination experiments by utilizing measured critical energy release rate values from the experiments. This integrated experimental-computational approach was validated by comparisons between simulation predicted and experimentally measured load-displacement response and delamination front shapes for the two types of experiments, which show good

agreement.

Delamination experiments and simulations facilitate quantification of the mechanical response of arterial walls and their behavior during various modes of delamination, leading to improved understanding of the patho-physiological mechanical performance of these tissues. Results of these efforts can shed light on the genesis and progression of pathological aortic dissections.

Acknowledgements

Research reported in this publication was supported by the National Science Foundation (NSF) under Award no. CMMI-1200358. This work was also partially supported by a SPARC Graduate Research Grant to Xiaochang Leng from the Office of the Vice President for Research at the University of South Carolina.

References

ABAQUS, 2013. Analysis User's Manual Version 6. Dassault Systemes Corp., pp. 12.
Bernard, Y., Zimmermann, H., Chocron, S., Litzler, J.-F., Kastler, B., Etievent, J.-P., Meneveau, N., Schiele, F., Bassand, J.-P., 2001. False lumen patency as a predictor of late outcome in aortic dissection. Am. J. Cardiol. 87, 1378–1382.
Camanho, P.P., Davila, C., De Moura, M., 2003. Numerical simulation of mixed-mode progressive delamination in composite materials. J. Compos. Mater. 37, 1415–1438.
Carson, M.W., Roach, M.R., 1990. The strength of the aortic media and its role in the propagation of aortic dissection. J. Biomech. 23, 579–588.
Chen, X., Deng, X., Sutton, M.A., 2013. Simulation of stable tearing crack growth events using the cohesive zone model approach. Eng. Fract. Mech. 99, 223–238.
Daugherty, A., Cassis, L., 2002. Mechanisms of abdominal aortic aneurysm formation. Curr. Atheroscler. Rep. 4, 222–227.
Ferrara, A., Pandolfi, A., 2010. A numerical study of arterial media dissection processes. Int. J. Fract. 166, 21–33.
Gasser, T.C., Holzapfel, G., 2007. Modeling plaque fissuring and dissection during balloon angioplasty intervention. Ann. Biomed. Eng. 35, 711–723.
Gasser, T.C., Holzapfel, G.A., 2006. Modeling the propagation of arterial dissection. Eur. J. Mech. – A/Solids 25, 617–633.
Gasser, T.C., Ogden, R.W., Holzapfel, G.A., 2006. Hyperelastic modelling of arterial layers with distributed collagen fibre orientations. J. R. Soc. Interface 3, 15–35.
Golledge, J., Norman, P., 2010. Atherosclerosis and abdominal aortic aneurysm: cause, response or common risk factors? Arterioscler. Thromb. Vasc. Biol. 30, 1075–1077.
Holzapfel, G.A., Gasser, T.C., Ogden, R.W., 2000. A new constitutive framework for arterial wall mechanics and a comparative study of material models. J. Elast. Phys. Sci. Solids 61, 1–48.
Leng, X., Chen, X., Deng, X., Sutton, M.A., Lessner, S.M., 2015a. Modeling of experimental atherosclerotic plaque delamination. Ann. Biomed. Eng. 43, 2838–2851.
Leng, X., Davis, L., Deng, X., Sutton, M.A., Lessner, S.M., 2015b. Numerical modeling of experimental human fibrous cap delamination. J. Mech. Behav. Biomed. Mater. 59, 322–336.
Ortiz, M., Pandolfi, A., 1999. Finite-deformation irreversible cohesive elements for three-dimensional crack-propagation analysis. Int. J. Numer. Methods Eng. 44, 1267–1282.
Prim, D.A., Zhou, B., Hartstone-Rose, A., Uline, M.J., Shazly, T., Eberth, J.F., 2016. A mechanical argument for the differential performance of coronary artery grafts. J. Mech. Behav. Biomed. Mater. 54, 93–105.
Roach, M.R., Song, S.H., 1994. Variations in strength of the porcine aorta as a function of location. Clin. Investig. Med. Med. Clin. Exp. 17, 308–318.
Roy, Y.A., Dodds Jr., R., 2001. Simulation of ductile crack growth in thin aluminum panels using 3-D surface cohesive elements. Int. J. Fract. 110, 21–45.
Sommer, G., Gasser, T.C., Regitnig, P., Auer, M., Holzapfel, G.A., 2008. Dissection properties of the human aortic media: an experimental study. J. Biomech. Eng. 130, 021007.
Tong, J., Sommer, G., Regitnig, P., Holzapfel, G.A., 2011. Dissection properties and mechanical strength of tissue components in human carotid bifurcations. Ann. Biomed. Eng. 39, 1703–1719.
Turon, A., Camanho, P.P., Costa, J., Dávila, C.G., 2006. A damage model for the simulation of delamination in advanced composites under variable-mode loading. Mech. Mater. 38, 1072–1089.
Venkatasubramaniam, A.K., Fagan, M.J., Mehta, T., Mylankal, K.J., Ray, B., Kuhan, G., Chetter, I.C., McCollum, P.T., 2004. A comparative study of aortic wall stress using finite element analysis for ruptured and non-ruptured abdominal aortic aneurysms. Eur. J. Vasc. Endovasc. Surg. 28, 168–176.
Wang, Y., Johnson, J.A., Fulp, A., Sutton, M.A., Lessner, S.M., 2013. Adhesive strength of atherosclerotic plaque in a mouse model depends on local collagen content and elastin fragmentation. J. Biomech. 46, 716–722.
Wang, Y., Johnson, J.A., Spinale, F.G., Sutton, M.A., Lessner, S.M., 2014. Quantitative measurement of dissection resistance in intimal and medial layers of human coronary arteries. Exp. Mech. 54, 677–683.
Wang, Y., Ning, J., Johnson, J.A., Sutton, M.A., Lessner, S.M., 2011. Development of a quantitative mechanical test of atherosclerotic plaque stability. J. Biomech. 44, 2439–2445.
Zhou, B., Rachev, A., Shazly, T., 2015. The biaxial active mechanical properties of the porcine primary renal artery. J. Mech. Behav. Biomed. Mater. 48, 28–37.
Zhou, B., Wolf, L., Rachev, A., Shazly, T., 2014. A structure-motivated model of the passive mechanical response of the primary porcine renal artery. J. Mech. Med. Biol. 14, 1450033.